Eur. Phys. J. A (2021) 57:330
https://doi.org/10.1140/epja/s10050-021-00639-w

THE EUROPEAN PHYSICAL JOURNAL A

Regular Article - Theoretical Physics

Collision centrality and system size dependences of light nuclei production via dynamical coalescence mechanism

Yi-Lin Cheng[1,2,3], **Song Zhang**[2,a], **Yu-Gang Ma**[2,b]

[1] Shanghai Institute of Applied Physics, Chinese Academy of Sciences, Shanghai 201800, China
[2] Key Laboratory of Nuclear Physics and Ion-beam Application (MOE), Institute of Modern Physics, Fudan University, Shanghai 200433, China
[3] School of Nuclear Sciences and Technology, University of Chinese Academy of Sciences, Beijing 100049, China

Received: 20 August 2021 / Accepted: 23 November 2021 / Published online: 14 December 2021

Communicated by Che-Ming Ko

Abstract Light (anti-)nuclei in relativistic heavy-ion collisions are considered to be formed by the coalescence mechanism of (anti-)nucleons in the present work. Using a dynamical phase-space coalescence model coupled with a multi-phase transport (AMPT) model, we explore the formation of light clusters such as deuteron, triton and their anti-particles in different centralities for ^{197}Au + ^{197}Au collisions at $\sqrt{s_{NN}} = 39$ GeV. The calculated transverse momentum spectra of protons, deuterons, and tritons are comparable to those of experimental data from the RHIC-STAR collaboration. Both coalescence parameters B_2 for (anti-)deuteron and B_3 for triton increase with the transverse momentum as well as the collision centrality, and they are comparable with the measured values in experiments. The effect of system size on the production of light nuclei is also investigated by ^{10}B + ^{10}B, ^{16}O + ^{16}O, ^{40}Ca + ^{40}Ca, and ^{197}Au + ^{197}Au systems in central collisions. The results show that yields of light nuclei increase with system size, while the values of coalescence parameters present an opposite trend. It is interesting to see that the system size, as well as the centrality dependence of B_A ($A = 2, 3$), falls into the same group, which further demonstrates production probability of light nuclei is proportional to the size of the fireball. Furthermore, we compare our coalescence results with other models, such as the thermal model and analytic coalescence model, it seems that the description of light nuclei production is consistent with each other.

1 Introduction

Quantum Chromodynamics (QCD) predicts that a new state of matter, namely the quark-gluon plasma (QGP), is likely to be formed in an extremely high temperature or density environment [1], which could be existed in the microseconds after the big bang. Studying this new matter is of great significance for us to have a comprehensive understanding not only of the basic composition and interaction of matter but also the information of the early evolution of the universe. Relativistic heavy-ion collision is currently considered as a unique way in the laboratory to detect such extremely high-temperature and -density QCD matter and then explore the QGP phase structure. However, the QGP state can only survive at a relatively short stage in the collision process, and it is soon hadronized as the system's temperature and density rapidly decrease, then hadrons will interact with each other. While hadronic interaction ceases, the particle approaches a kinetic freeze-out stage. Experimentally one can infer the properties of the early QGP by exploring the kinetic freeze-out particles. Therefore, exploring the properties of QGP and QCD critical point from the regular hadronic matter to the QGP phase remains of great interest to the field [2–9].

Considering the light nuclei have small binding energy, it is also an open question of how they can survive from the hot nuclear matter. They might be disintegrated and regenerated through the coalescence of nucleons which are de-coupled from the hot and dense system, so the production of light nuclei can be used to extract the information of freeze-out nucleon distributions [10] and to understand how the QGP expands, cools and hadronizes. These pieces of information provide crucial insights for dynamical mechanism and space-time evolution of heavy-ion collisions [11–15]. Recently the light nucleus also demonstrates its significance to search for the possible critical point in the phase diagram of strongly

[a] e-mail: song_zhang@fudan.edu.cn
[b] e-mail: mayugang@fudan.edu.cn (corresponding author)

interacting quark matter [16–21]. Theoretical study about the light clusters has been undertaken for a long time and several models or methods are used to explore the production of light nuclei. Thermal models [22–25] have successfully described the yields of hadrons and nuclei. Besides, the coalescence model has been used to describe the production of light nuclei for many years [26–32]. These calculations by using a similar coalescence mechanism coupled with phase-space distribution from different models, such as blast-wave model and transport model, seem to resemble each other of description for light nuclei production at RHIC and LHC energies. The production of light nuclei can be also described by the kinetic equations [33,34]. Especially recently, the relativistic kinetic equations with their nonlocal collision integrals were also solved for successfully describing light (anti-)nuclei production from the many-body scatterings in high-energy nuclear collisions [35].

In the present work, the system size dependence (centrality and collision system) are payed more attention. We investigate the production of deuteron and triton in relativistic heavy-ion collision by means of A Multi-Phase Transport (AMPT) model [36] followed by a dynamical coalescence model for ^{197}Au + ^{197}Au collisions at different centralities as well as for the central collisions of ^{10}B + ^{10}B, ^{16}O + ^{16}O, and ^{40}Ca + ^{40}Ca at $\sqrt{s_{NN}} = 39$ GeV. The coalescence factor extracted from the transverse momentum spectra of light nuclei and proton represents the coalescence probability, and it is related to the source volume that decreases with the increasing of constituent momentum of coalesced nucleons [37]. The transverse momentum (p_T) distribution and the coalescence parameters (B_A) of light nuclei are comparable to the experimental data. On the other hand, the properties of QGP are sensitive to the initial geometry and the dynamical fluctuations in heavy-ion collisions, and the system size scan experiment has been proposed at RHIC energies recently [38]. These experiments will provide us more information of the initial geometry distribution and fluctuation effects on momentum distribution at the final stage, and some related theoretical analytical works have been performed [24,39–44]. Along this direction, a system scan of the coalescence parameters is undertaken in the present work and it is found that B_A falls into the same group for its centrality dependence when both the system size and centrality are expressed by charged particle multiplicity ($\langle N_{ch} \rangle$) including $\pi^{\pm}$, $k^{\pm}$, p, $\bar{p}$, which indicates that light nuclei production essentially depends on the size of the fireball.

The paper is arranged as follows: In Sect. 2, a brief description of the AMPT model which is used to generate the nucleon phase-space distribution at the freeze-out stage is presented. Also,the coalescence model for the light cluster is described, including the Wigner phase space density functions for the (anti)deuteron and (anti)triton. In Sect. 3, the results of p_T distribution and the coalescence parameters of (anti)deuteron and triton from ^{10}B + ^{10}B, ^{16}O + ^{16}O and ^{40}Ca + ^{40}Ca in central collisions as well as ^{197}Au + ^{197}Au collisions at different centralities are compared to the available experimental data. Finally, a conclusion is presented in Sect. 4.

2 Model and algorithms

2.1 AMPT model

A multi-phase transport model [36] was used to provide the phase-space of nucleons in this work. The model is composed of four parts: the HIJING model [45,46] is used to simulate the initial conditions, the Zhang's Parton Cascade (ZPC) model [47] is employed to describe partonic interaction, the Lund string fragmentation or coalescence model is used for the hadronization process, and A Relativistic Transport (ART) model [48] is applied to describe the hadronic rescattering process. As an event generator used in this work, the AMPT model outputs the phase-space distribution at the final stage in the hadronic rescattering process (ART model [48]) with considering baryon-baryon, baryon-meson, and meson-meson elastic and inelastic scatterings, as well as resonance decay or weak decay. In Refs. [36,48] the interaction cross section was presented and extended. The hadronic rescattering time would affect light nuclei spectra and yield which are based on the phase-space information of nucleons from the AMPT model. Refs. [36,49] suggest the maximum hadronic rescattering time ($t_{max,h}$), which means to cease a hadron interacting with others if it still dose not reach freeze-out state at that time, 30 fm/c for the RHIC energy region and 200 fm/c for the LHC energy region. Here the p_T spectra of p, d and t with the cutoff of the maximum hadronic rescattering time of 30 fm/c and 100 fm/c are checked. Figure 1 shows the p_T spectra of proton, deuteron and triton of ^{197}Au + ^{197}Au collisions at mid-rapidity ($|y| < 0.5$) for different centralities at $\sqrt{s_{NN}} = 39$ GeV, and Fig. 2 presents the p_T results for the 0−10% central collisions of ^{10}B + ^{10}B, ^{16}O + ^{16}O, ^{40}Ca + ^{40}Ca at $\sqrt{s_{NN}} = 39$ GeV and mid-rapidity ($|y| < 0.5$). We can find that these two cases are very close to each other. Afterwords we choose the case of $t_{max,h} = 100$ fm/c for the following calculations. We would mention that the AMPT model has been successfully used to simulate physics in heavy-ion collisions at the RHIC and LHC energies [36,49,50] and the detailed parameter configurations can be found therein.

2.2 Dynamical coalescence model

In the coalescence model [51], the invariant yields of light nuclei with charge number Z and atomic mass number A can be described by the yields of cluster constituents (protons and

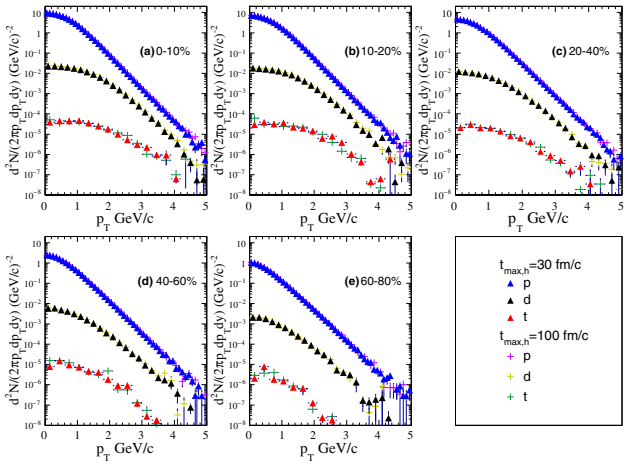

Fig. 1 Transverse momentum p_T spectra at mid-rapidity ($|y| < 0.5$) of proton, deuteron and triton in ^{197}Au + ^{197}Au collisions for different centralities at $\sqrt{s_{NN}} = 39$ GeV with the maximum hadronic rescattering time of 30 fm/c and 100 fm/c

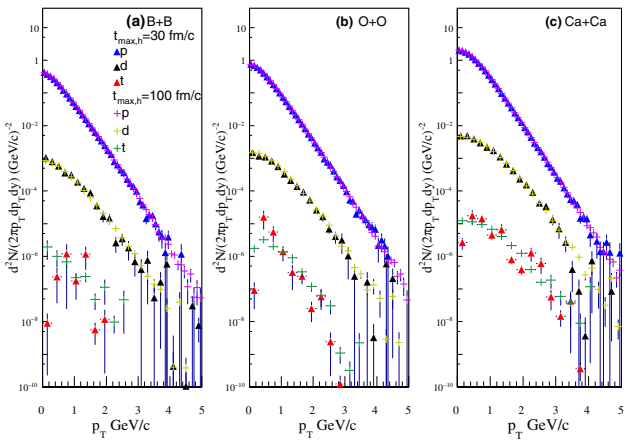

Fig. 2 Transverse momentum p_T spectra at mid-rapidity ($|y| < 0.5$) for 0−10% central collisions of ^{10}B + ^{10}B, ^{16}O + ^{16}O, ^{40}Ca + ^{40}Ca systems at $\sqrt{s_{NN}} = 39$ GeV with the maximum hadronic rescattering time of 30 fm/c and 100 fm/c

neutrons) multiplying by a coalescence parameter B_A,

$$E_A\frac{d^3N_A}{dp_A^3} = B_A\left(E_p\frac{d^3N_p}{dp_p^3}\right)^Z\left(E_n\frac{d^3N_n}{dp_n^3}\right)^{A-Z} \approx B_A\left(E_p\frac{d^3N_p}{dp_p^3}\right)^A, \quad (1)$$

where p_p and p_n are the momenta of proton and neutron, respectively, and p_A is the momentum of the nucleus with the mass number A which is approximate A times of proton momentum, i.e. Ap_p, assuming that the distributions of neutrons and protons are the same. The coalescence parameter B_A related to the local nucleon density reflects the probability of nucleon coalescence. The coalescence parameter B_A is also related to the effective volume of the nuclear matter at the time of coalescence of nucleons into light nuclei, called nucleon correlation volume V_{eff} [51], i.e. $B_A \propto 1/V_{eff}^{A-1}$.

The dynamical coalescence model can give the probability of light nuclei (M-nucleon cluster) by the overlap of the cluster Wigner phase-space density with the nucleon phase-space distributions at an equal time in the M-nucleon rest frame at the freeze-out stage [52]. The momentum distribution of a cluster in a system containing A nucleons can be expressed by,

$$\frac{d^3N_M}{d^3K} = G\binom{A}{M}\binom{M}{Z}\frac{1}{A^M}\int\left[\prod_{i=1}^{Z}f_p(\vec{r}_i,\vec{k}_i)\right]\left[\prod_{i=Z+1}^{M}f_n(\vec{r}_i,\vec{k}_i)\right]\times\rho^W(\vec{r}_{i_1},\vec{k}_{i_1},\cdots,\vec{r}_{i_{M-1}},\vec{k}_{i_{M-1}}) \times\delta(\vec{K}-(\vec{k}_1+\cdots+\vec{k}_M))d\vec{r}_1d\vec{k}_1\cdots d\vec{r}_Md\vec{k}_M, \quad (2)$$

where M and Z are the number of the nucleon and proton of the cluster, respectively; f_n and f_p are the neutron and proton phase-space distribution functions at freeze-out, respectively; ρ^W is the Wigner density function; $\vec{r}_{i_1},\cdots,\vec{r}_{i_{M-1}}$ and $\vec{k}_{i_1},\cdots,\vec{k}_{i_{M-1}}$ are the relative coordinates and momentum in the M-nucleon rest frame; the spin-isospin statistical factor G is 3/8 for deuteron and 1/3 for triton [52], note whether to consider the isospin effect is still an unresolved problem, neglecting the isospin effect can be found in [53,54]. While the neutron and proton phase-space distribution comes from the transport model simulations, the multiplicity of a M-nucleon cluster is then given by,

$$N_M = G\int\sum_{i_1>i_2>\cdots>i_M}d\vec{r}_{i_1}d\vec{k}_{i_1}\cdots d\vec{r}_{i_{M-1}}d\vec{k}_{i_{M-1}} \langle\rho_i^W(\vec{r}_{i_1},\vec{k}_{i_1},\cdots,\vec{r}_{i_{M-1}},\vec{k}_{i_{M-1}})\rangle, \quad (3)$$

where the $\langle\cdots\rangle$ denotes the event averaging.

2.3 Wigner phase-space density

The Wigner phase-space density of (anti)deuteron is assumed as [52],

$$\rho_d^W(\vec{r},\vec{k}) = 8\sum_{i=1}^{15}c_i^2\exp\left(-2\omega_i r^2-\frac{k^2}{2\omega_i}\right) +16\sum_{i>j}^{15}c_ic_j\left(\frac{4\omega_i\omega_j}{(\omega_i+\omega_j)^2}\right)^{\frac{3}{4}}\exp\left(-\frac{4\omega_i\omega_j}{\omega_i+\omega_j}r^2\right) \times\exp\left(-\frac{k^2}{\omega_i+\omega_j}\right)\cos\left(2\frac{\omega_i-\omega_j}{\omega_i+\omega_j}\vec{r}\cdot\vec{k}\right), \quad (4)$$

where the Gaussian fit coefficient c_i and w_i are given in Ref. [52]. $\vec{k} = (\vec{k}_1\text{-}\vec{k}_2)/2$ is the relative momentum and

$\vec{r}$ = ($\vec{r}_1$-$\vec{r}_2$) is the relative coordinate of proton and neutron inside deuteron.

The Wigner phase-space density of triton is obtained from a spherical harmonic oscillator [28,52,55],

$$\begin{aligned}\rho_t^W(\rho,\lambda,\vec{k}_\rho,\vec{k}_\lambda) &= \int \psi\left(\rho+\frac{\vec{R}_1}{2},\lambda+\frac{\vec{R}_2}{2}\right)\psi^*\left(\rho-\frac{\vec{R}_1}{2},\lambda-\frac{\vec{R}_2}{2}\right) \\ &\quad\times\exp(-i\vec{k}_\rho\cdot\vec{R}_1)\exp(-i\vec{k}_\lambda\cdot\vec{R}_2)3^{\frac{3}{2}}d\vec{R}_1d\vec{R}_2 \\ &= 8^2\exp\left(-\frac{\rho^2+\lambda^2}{b^2}\right)\exp\left(-\left(\vec{k}_\rho^2+\vec{k}_\lambda^2\right)b^2\right),\end{aligned} \tag{5}$$

where ρ and λ are relative coordinates, $\vec{k}_\rho$ and $\vec{k}_\lambda$ are the relative momenta in the Jacobi coordinate, the parameter b is obtained from the root-mean-square radius, 1.61 fm for triton [52].

In practice, the coalescence procedure by using Eq. (3) can not guarantee the energy conservation, such as for the formation of dueteron $p+n\rightarrow d$. If a proton and a neutron with momentum-energy $(\vec{k},E_p)$ and $(-\vec{k},E_n)$ coalesces a deuteron with $(\vec{0},m_d)$, and then the lost energy is $\Delta E = \sqrt{k^2+m_p^2}+\sqrt{k^2+m_n^2}-m_d$. From Eq. (4), it can be seen that the lost energy is ignorable since the Wigner density is suppressed exponentially at the large relative momentum. For the three-body case, a similar derivation can be obtained. Actually, we made a numerical check for the effect of lost energy, it is found that it is negligible for the yield and spectra of the light nuclei production.

In this calculation, the AMPT model provides the phase-space of nucleons at the freeze-out stage in heavy-ion collisions and the followed coalescence model is coupled to give the transverse momentum p_T spectra of deuterons (d) and tritons (t). Based on the obtained p_T spectra, the yields of d and t, as well as the coalescence parameters, are discussed.

3 Results and discussion

To discuss the system size dependence of light nuclei production, some quantities of the collision systems are shown in Fig. 3, such as $\langle N_{part}\rangle$ representing the average number of participants, and $\langle N_{ch}\rangle$ denoting the average number of charged hadrons ($\pi^\pm$, $k^\pm$, p, $\bar{p}$) with a kinetic window of $0.2<p_T<2$ GeV/c and rapidity $|y|<0.5$ (mid-rapidity), $\sqrt{\langle r_i^2\rangle}$ representing the averaged radius of the initial collision zone which is calculated through the participants, $\sqrt{\langle r_f^2\rangle}$ representing the averaged radius of the collision system at freeze-out stage which is calculated through the charged hadrons. It is seen that $\langle N_{part}\rangle$ and $\langle N_{ch}\rangle$ are all proportional to collision system size at final stage, namely $\sqrt{\langle r_f^2\rangle}$,

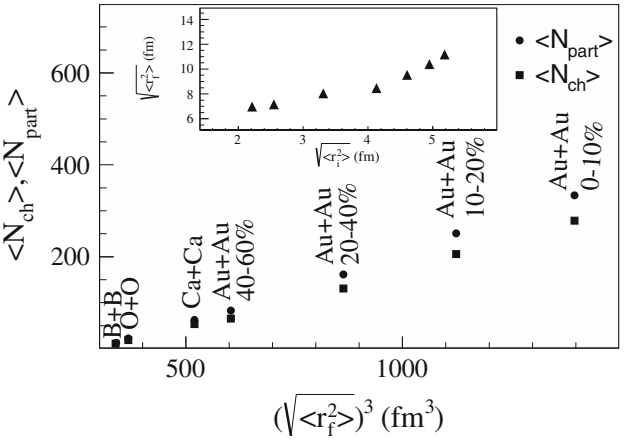

Fig. 3 Relationship between $\langle N_{part}\rangle$ ($\langle N_{ch}\rangle$) and $\sqrt{\langle r_f^2\rangle}$ to characterise the system size. The insert plots a correlation between $\sqrt{\langle r_i^2\rangle}$ and $\sqrt{\langle r_f^2\rangle}$

for different collision systems. In the insert, the freeze-out radius of the collision system $\sqrt{\langle r_f^2\rangle}$ increases with the initial radius of the collision zone, namely $\sqrt{\langle r_i^2\rangle}$. So both $\langle N_{part}\rangle$ and $\langle N_{ch}\rangle$ can characterise the collision system size, and it is therefore convenient to discuss system size dependence of observables by comparing the $\langle N_{ch}\rangle$ -dependent results with experimental data in the following.

3.1 p_T spectra of p ($\bar{p}$), d ($\bar{d}$) and t ($\bar{t}$)

Figure 4 presents the transverse momentum spectra of p ($\bar{p}$), d ($\bar{d}$) and t ($\bar{t}$) calculated by the AMPT model coupling with the coalescence model in Au + Au collisions at $\sqrt{s_{NN}}=39$ GeV. The results are shown for the collision centrality classes of 0–5%, 5–10%, 10–20%, 20–30%, 30–40%, 40–50%, 50–60%, and 60–70% for p ($\bar{p}$) in Fig. 4a, d, 0–10%, 10–20%, 20–40%, 40–60%, and 60–80% for d ($\bar{d}$) in Fig. 4b, e, 0–10%, 10–20%, 20–40%, and 40–80% for t ($\bar{t}$) in Fig. 4c, f. It is found that the results can well describe the experimental data for p [56], d [10] and t [57] spectra from the STAR collaboration, especially in central collisions. Besides, we compared the transverse momentum spectra of p ($\bar{p}$), d ($\bar{d}$) and t with the results from the iEBE-MUSIC hybrid model plus coalescence model [31]. Note that the isospin effect in the statistical factor in Eq. (2) can result in a constant factor among the results [31,54] and does not affect the shape of the spectra. It is interesting to see that two models are consistent, which implies that the phase-space of the two models have similar properties or distributions.

Figure 5 shows the calculated transverse momentum spectra for p ($\bar{p}$) ((a) and (b)), d ($\bar{d}$) ((c) and (d)) and t ($\bar{t}$) ((e) and (f)) in ^{10}B + ^{10}B, ^{16}O + ^{16}O, ^{40}Ca + ^{40}Ca, and ^{197}Au

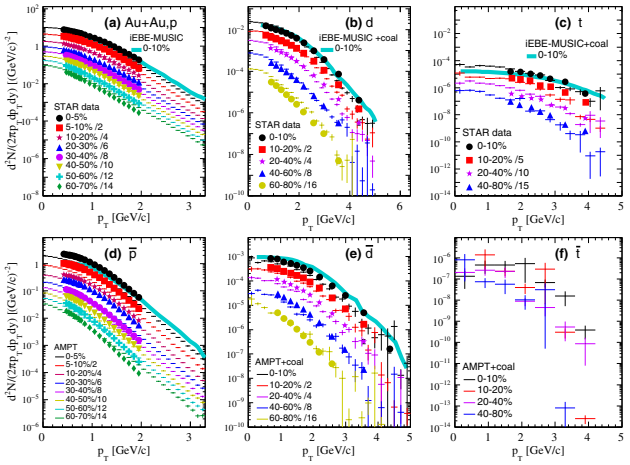

Fig. 4 Transverse momentum p_T spectra at mid-rapidity ($|y| < 0.5$) of (anti)proton, (anti)deuteron and (anti)triton in ^{197}Au + ^{197}Au collisions for different centralities at $\sqrt{s_{NN}} = 39$ GeV. Solid markers represent the experimental data from the STAR collaboration [10,56,57] and lines represent the model calculation results. The smooth lines represent the results of (anti)proton from the iEBE-MUSIC hybrid model, (anti)deuteron and triton from the iEBE-MUSIC hybrid model plus the coalescence model [31]

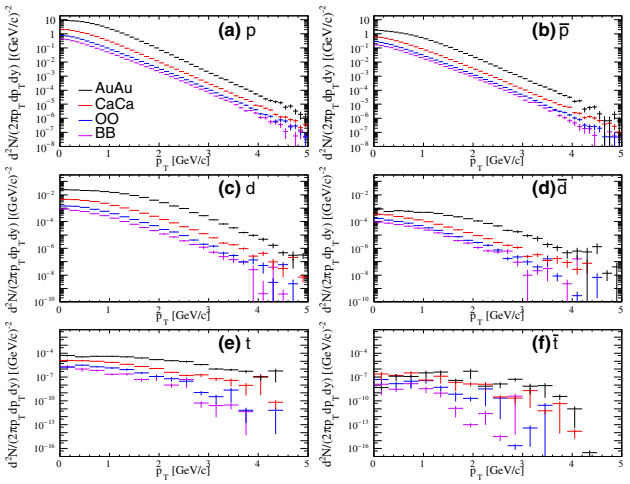

Fig. 5 Transverse momentum p_T spectra at mid-rapidity ($|y| < 0.5$) of (anti)proton, (anti)deuteron and (anti)triton in 0−10% central collisions of ^{10}B + ^{10}B, ^{16}O + ^{16}O, ^{40}Ca + ^{40}Ca, and ^{197}Au + ^{197}Au at $\sqrt{s_{NN}} = 39$ GeV by using the AMPT model coupling with the coalescence model

+ ^{197}Au in 0−10% central collisions at $\sqrt{s_{NN}} = 39$ GeV. The p_T spectra present an obvious collision system dependence in central collisions and drop with the decreasing of the collision system size [58].

3.2 $\langle dN/dy \rangle$ of p ($\bar{p}$), d ($\bar{d}$) and t ($\bar{t}$)

The rapidity densities ($\langle dN/dy \rangle$) of p ($\bar{p}$), d ($\bar{d}$) and t ($\bar{t}$) are calculated in mid-rapidity as a function of $\langle N_{ch} \rangle$ in ^{10}B + ^{10}B, ^{16}O + ^{16}O, ^{40}Ca + ^{40}Ca, and ^{197}Au + ^{197}Au collisions at $\sqrt{s_{NN}} = 39$ GeV, as shown in Fig. 6. It is found that $\langle dN/dy \rangle$ of p as a function of $\langle N_{ch} \rangle$ (Fig. 6a) can well describe the data [56] but underestimate $\bar{p}$ data in Au + Au collisions at $\sqrt{s_{NN}} = 39$ GeV. For d and $\bar{d}$ (Fig. 6b), it presents the similar description quality to the data [10]. $\langle dN/dy \rangle$ of t and $\bar{t}$ as a function of $\langle N_{ch} \rangle$ is presented in Fig. 6c. As shown in Fig. 6a, b, $\langle dN/dy \rangle$ of p and d are comparable to those from the iEBE-MUSIC hybrid model plus coalescence model [31] in central collisions, and little difference for anti-matter partners. In addition, the yields of these light (anti)nuclei for the 0-10% central collisions of ^{10}B + ^{10}B, ^{16}O + ^{16}O, and ^{40}Ca + ^{40}Ca systems at $\sqrt{s_{NN}} = 39$ GeV are also shown in Fig. 6, and it seems that they follow the similar $\langle N_{ch} \rangle$ systematics. In general, it is reasonably speculated that $\langle dN/dy \rangle$ of (anti)proton, (anti)deuteron and triton present an increasing trend with $\langle N_{ch} \rangle$ (collision system size) in different collision centralities as well as collision systems.

Furthermore, we calculate the $\langle N_{ch} \rangle$ dependence of ratios of d/p and t/p by using a thermal model [59],

$$n_i(T, \vec{\mu}) = \frac{\langle N_i \rangle}{V} = \frac{T g_i}{2\pi^2} \sum_{k=1}^{\infty} \frac{(\pm 1)^{k+1}}{k} \lambda_i^k m_i^2 K_2 \left(\frac{k m_i}{T} \right), \quad (6)$$

where $\lambda_i(T, \vec{\mu}) = \exp(\frac{B_i \mu_B + S_i \mu_s + Q_i \mu_Q}{T})$, B_i, S_i and Q_i are the baryon number, strangeness number and charge number, μ_B, μ_S and μ_Q, are their corresponding chemical potentials of particle i, K_2 is the modified Bessel function and the upper sign is for bosons and lower for fermions, g_i is the spin−isospin degeneracy factor. We use the parameters such as the chemical freeze-out temperature as well as the baryon chemical potential from Ref. [56]. As shown in Fig. 6d, the d/p and t/p ratios of AMPT + coalescence model are bigger than STAR data [10,56,60]. And the d/p ratio from the thermal model can describe the STAR data [10,56,60] but overestimates the t/p ratio, which is consistent with the results in references [60–62].

Figure 7 presents a comparison between $\langle N_{ch} \rangle$ dependence of the fireball radius ($\sqrt{\langle r_f^2 \rangle}$) calculated directly by the coordinates from the AMPT model and that r_V from the analytic coalescence model [63] in ^{197}Au + ^{197}Au collisions at $\sqrt{s_{NN}} = 39$ GeV. In analytic coalescence model [63], a blast-wave-like parametrization is used for the phase-space configuration of constituent particles at freeze-out. We extract the effective volume by equation (25) in Ref. [63], then the fireball radius r_V can be calculated by assuming a spherical fireball. We find that the both radii ($\sqrt{\langle r_f^2 \rangle}$ and r_V) present a similar $\langle N_{ch} \rangle$ dependence, i.e. increasing as $\langle N_{ch} \rangle$. Of course, we notice that the values of size have model or calculation method dependence.

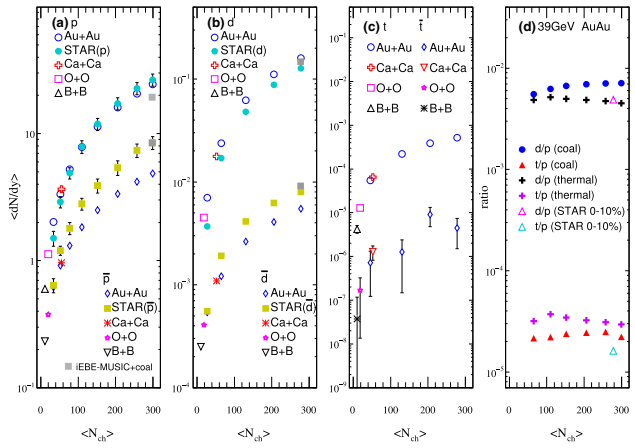

Fig. 6 $\langle N_{ch}\rangle$ dependence of the yield $\langle dN/dy\rangle$ of p ($\bar{p}$), d ($\bar{d}$) and t ($\bar{t}$) from ^{10}B + ^{10}B, ^{16}O + ^{16}O, ^{40}Ca + ^{40}Ca, and ^{197}Au + ^{197}Au collision systems at 0−10% centrality and $\sqrt{s_{NN}}$ = 39 GeV are presented in (a)-(c). Results are compared with experimental data of p ($\bar{p}$) and d ($\bar{d}$) in ^{197}Au + ^{197}Au collisions at $\sqrt{s_{NN}}$ = 39 GeV [10,56]. The gray markers are the results of the iEBE-MUSIC hybrid model plus coalescence model [31]. The comparison of $\langle dN/dy\rangle$ dependence of d/p and t/p between coalescence model and thermal model (fitted parameters is from Ref. [56]) and the STAR data [54,56] are shown in (d)

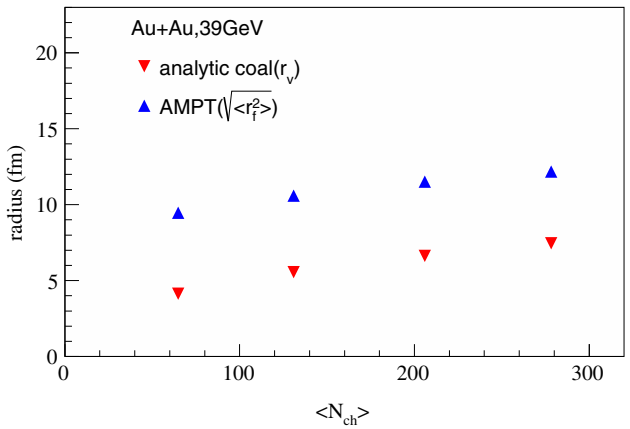

Fig. 7 The comparison of $\langle N_{ch}\rangle$ dependence of the fireball radius calculated directly from coordinates in the AMPT calculations as well as the results obtained by analytic coalescence model [63] in ^{197}Au + ^{197}Au collisions at $\sqrt{s_{NN}}$ = 39 GeV

Figure 8a shows the $\langle dN/dy\rangle$ of proton, deuteron and triton as a function of baryon number B from the coalescence model in 0–10% ^{10}B + ^{10}B, ^{16}O + ^{16}O, and ^{40}Ca + ^{40}Ca collisions, as well as the 0–10%, 10–20%, 20–40%, 40–60%, and 60–80% ^{197}Au + ^{197}Au collisions at $\sqrt{s_{NN}}$ = 39 GeV. The lines are the fits to the calculated results by a function of $N_0 e^{-rB}$, here N_0 denotes amplitude, B is the baryon number and r is the reduction factor. It is found that the yields of proton, deuteron ,and triton in each collision system exhibit a decreasing exponential trend with the baryon number. The reduction factor [55,64] by fitting the yields of proton, deuteron and triton as a function of $\langle N_{ch}\rangle$ is shown

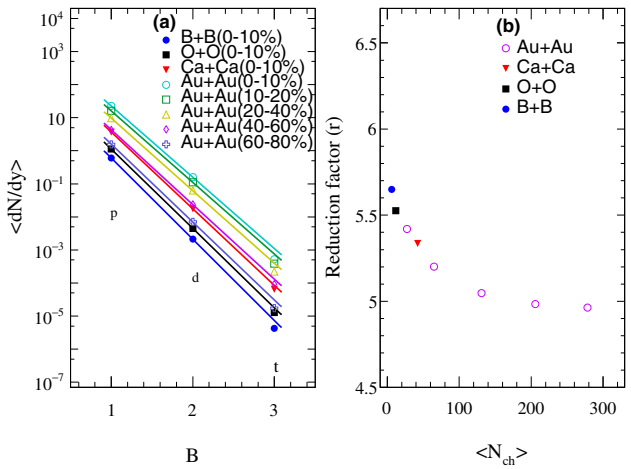

Fig. 8 **a** The yields of proton, deuteron, and triton as a function of baryon number B from the coalescence model for the 0–10% ^{10}B + ^{10}B, ^{16}O + ^{16}O, and ^{40}Ca + ^{40}Ca collisions, as well as for the 0–10%, 10–20%, 20-40%, 40–60%, and 60–80% ^{197}Au + ^{197}Au collisions at $\sqrt{s_{NN}}$ = 39 GeV, (**b**) the extracted reduction factor r obtained by fitting the yields of proton, deuteron, and triton with a function of $N_0 e^{-rB}$ versus $\langle N_{ch}\rangle$

in Fig. 8b. While the system size is expressed by $\langle N_{ch}\rangle$, the reduction factor decreases sharply with the increasing of $\langle N_{ch}\rangle$ and then saturate at large $\langle N_{ch}\rangle$. This implies that light nuclei production becomes more difficult in small systems, especially for that with baryon number B >3 in the relativistic heavy-ion collisions.

3.3 Coalescence parameters B_2 and B_3

To further characterize the system size dependence of light nuclei production, the coalescence probability of forming light clusters is investigated by the coalescence parameters B_A (A = 2 and 3) as defined in Eq. (1). In panel (a) and (b) of Fig. 9, the calculated coalescence parameter B_2 are compared with the data measured by the STAR collaboration [10] in ^{197}Au + ^{197}Au collisions at RHIC energy of 39 GeV in 0–10%, 10–20%, 20–40%, and 40–60% (40–80% for triton) centralities. The calculated results present a similar trend with the experimental data, the coalescence parameters B_2 in panel (a), (b) and B_3 in panel (c) as a function of p_T/A in different collision centralities always present an increasing trend, this might be due to the increasing correlation volume with the decreasing of p_T, leading to a higher coalescence probability for larger p_T values. In addition, the values of B_2 and B_3 decrease with collision centrality (i.e. the more central collisions the less B_A), which suggests that source volume being larger in central collisions. From the viewpoint of the coalescence probability of nucleons to form these light clusters, it is reasonable to have a bigger coalescence probability while the distance between the protons and neutrons is smaller. On the other hand, we note that the val-

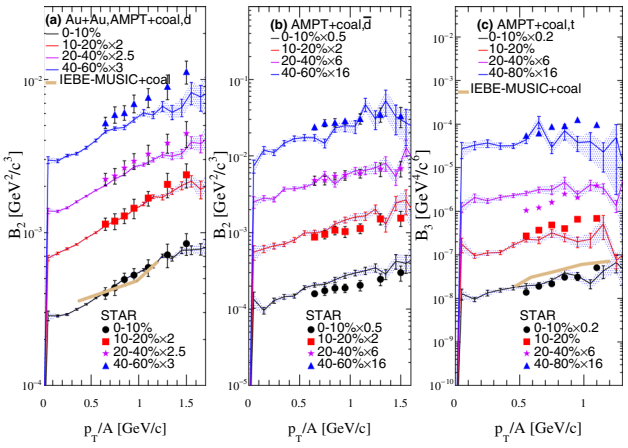

Fig. 9 Coalescence parameters B_2 and B_3 as a function of p_T/A for deuterons (**a**), anti-deuterons (**b**) and tritons (**c**) for ^{197}Au + ^{197}Au collisions at $\sqrt{s_{NN}}$ = 39 GeV at different centralities: 0–10%, 10–20%, 20–40%, and 40–60% (40–80% for t). The solid markers are experimental data of (anti)deuterons and tritons from the STAR collaboration [10]. The smooth lines are the results of B_2 and B_3 from the iEBE-MUSIC hybrid model plus coalescence model [31]

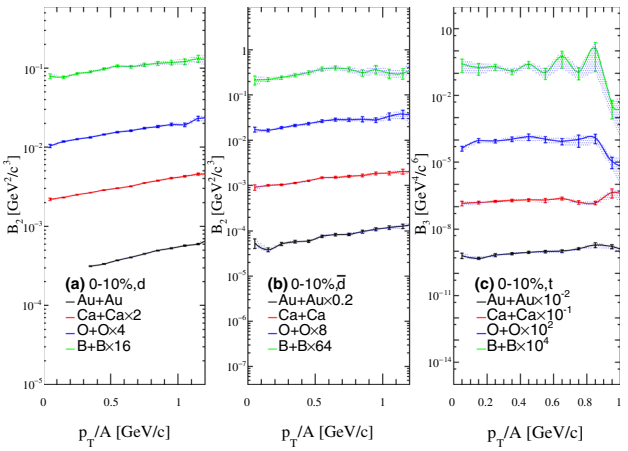

Fig. 10 Coalescence parameters B_2 and B_3 as a function of p_T/A for deuterons (**a**), anti-deuterons (**b**) and tritons (**c**) from 0 to 10% central collisions of ^{10}B + ^{10}B, ^{16}O + ^{16}O, ^{40}Ca + ^{40}Ca, and ^{197}Au + ^{197}Au at $\sqrt{s_{NN}}$ = 39 GeV

ues of B_2 for deuterons are systematically larger than those of anti-deuterons in the same centrality, it is consistent with the experimental observation [10], indicating that the correlated volume of baryons is smaller than that of anti-baryons. Besides, the comparison of our results of B_2 and B_3 with the iEBE-MUSIC hybrid model plus coalescence model [31] is also shown in this figure, and the trend remains similar.

Furthermore, the coalescence parameter B_2 for (anti)deuterons as a function of p_T/A is also calculated for ^{10}B + ^{10}B, ^{16}O + ^{16}O, and ^{40}Ca + ^{40}Ca collisions at 0–10% centrality at $\sqrt{s_{NN}}$ = 39 GeV, and the results are presented in Fig. 10 (a) and (b). It is found that the coalescence parameter B_2 presents a system size dependence, i.e. B_2 decreases as

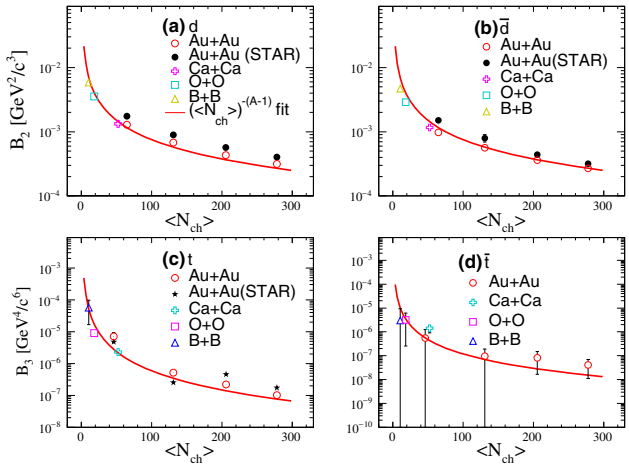

Fig. 11 $\langle N_{ch}\rangle$ dependence of B_2 and B_3 for the (anti)deuteron and (anti)triton in ^{197}Au + ^{197}Au collisions at 0–10%, 10–20%, 20–40%, and 40–60% centralities as well as the 0–10% central collisions of ^{10}B + ^{10}B, ^{16}O + ^{16}O and ^{40}Ca + ^{40}Ca systems at $\sqrt{s_{NN}}$ = 39 GeV. The experimental data of (anti)deuteron produced in ^{197}Au + ^{197}Au collision is taken from the STAR collaboration [10]

the system size increases. This result is consistent with the centrality dependence in the same system such as Au + Au collisions. The p_T dependence of B_2 also presents an upward trend as shown in Fig. 9. The coalescence parameter B_3 is presented as a function of p_T/A for the 0–10% central collisions of ^{10}B + ^{10}B, ^{16}O + ^{16}O, ^{40}Ca + ^{40}Ca, and ^{197}Au + ^{197}Au systems at $\sqrt{s_{NN}}$ = 39 GeV in Fig. 10c, it shows the similar trend with B_2 even though the error remains larger.

Figure 11 shows the $\langle N_{ch}\rangle$ dependence of coalescence parameters B_2 and B_3 of d ($\bar{d}$) (**a**, **b**), t ($\bar{t}$) (**c**, **d**) in ^{197}Au+^{197}Au collisions at 0–10%, 10–20%, 20–40%, and 40–60% (40–80% for t) centralities as well as 0–10% central collisions of ^{10}B + ^{10}B, ^{16}O + ^{16}O, ^{40}Ca + ^{40}Ca systems at $\sqrt{s_{NN}}$ = 39 GeV. It is observed that the coalescence parameters B_2 and B_3 present an obvious collision centrality dependence, the values of B_2 for deuteron and anti-deuteron decrease with the increasing of $\langle N_{ch}\rangle$. The $\langle N_{ch}\rangle$ dependence of B_3 for triton in ^{197}Au + ^{197}Au collisions at 0–10%, 10–20%, 20–40%, and 40–80% centralities at $\sqrt{s_{NN}}$ = 39 GeV is also shown in this figure. B_3 also shows a decreasing trend with $\langle N_{ch}\rangle$. Besides, it is observed that the values of B_2 and B_3 present an obvious collision system dependence in 0–10% central collisions of ^{10}B + ^{10}B, ^{16}O + ^{16}O, ^{40}Ca + ^{40}Ca, and ^{197}Au + ^{197}Au systems, the values of B_2 and B_3 for deuteron and anti-deuteron drop with the increasing of system size, the value of B_3 also shows a decreasing trend with $\langle N_{ch}\rangle$. Considering the properties of system size dependence from Fig. 3 as well as the relationship between coalescence parameter and nucleon correlation volume, i.e. $B_A \propto 1/V_{eff}^{A-1}$ [51], we found that B_A can be expressed by a simple function, $B_A \propto 1/(\langle N_{ch}\rangle)^{(A-1)}$ (here $A = 2$ or 3). From the viewpoint of light nuclei production by coalescence mechanism, it is

concluded that the coalescence parameter B_A can reflect the collision system size when the system is at kinetic freeze-out stage.

The thermal model has been successfully used to describe the multiplicities or particle ratios of hadrons and light nuclei [65] in relativistic heavy-ion collisions, while the coalescence model basing on phase space data is another useful tool to treat light nuclei production. In practice, the phase-space data can be generated from various models, such as blast-wave model [66], hydrodynamics [31], transport model [67] or pure analytical calculation [63]. In our work, the coalescence model basing on the AMPT phase space data is used to study the light nuclei production at RHIC lower energy in the Beam Energy Scan project [56,68], the results are consistent with the previous calculations and provide a more comprehensive understanding of the experiment data. Therefore we argue that these models could approach an equivalent simulation of the production of light nuclei assuming the thermal or kinetic freeze-out properties of the collision systems, respectively.

4 Summary

In summary, based on the AMPT model coupled with the dynamic coalescence model, the collision system size dependence of light nuclei production was investigated for the 0–10%, 10–20%, 20–40%, 40–60%, and 60–80% ^{197}Au + ^{197}Au collisions at $\sqrt{s_{NN}} = 39$ GeV. The calculated transverse momentum p_T spectra can well describe the experimental data from the STAR collaboration and the extracted coalescence parameters of B_2 and B_3 fitted the data well. In the same way, the production of light nuclei is also calculated for the 0–10% central collisions of ^{10}B + ^{10}B, ^{16}O + ^{16}O, and ^{40}Ca + ^{40}Ca systems at $\sqrt{s_{NN}} = 39$ GeV. As the system size is denoted by $\langle N_{ch}\rangle$ for different centralities and collision systems, the yields of light nuclei $\langle dN/dy\rangle$ present an obvious system size dependence, namely $\langle dN/dy\rangle$ increases with the system size ($\langle N_{ch}\rangle$). The reduction factor for light nuclei production is also presented for the system size dependence, which indicates that light nuclei production becomes more difficult in small systems. And the coalescence parameters B_A ($A = 2, 3$) as a function of $\langle N_{ch}\rangle$ fall into the same group regardless for different centralities in a fixed collision system or different systems at a fixed centrality. Coalescence parameters B_A ($A = 2, 3$) present a decreasing trend with the increasing of $\langle N_{ch}\rangle$, i.e. follow a proportional dependence on $1/\langle N_{ch}\rangle^{A-1}$. We can conclude that the light nucleus production essentially depends on the fireball volume, reflected in the system size or centralities. These results shed light on further experimental system scan project at RHIC or LHC.

Acknowledgements This work was supported in part by the National Natural Science Foundation of China under contract Nos. 11875066, 11890710, 11890714, 11925502, 11961141003, National Key R&D Program of China under Grant No. 2018YFE0104600 and 2016YFE0100900, the Strategic Priority Research Program of CAS under Grant No. XDB34000000, the Key Research Program of Frontier Sciences of the CAS under Grant No. QYZDJ-SSW- SLH002, and the Guangdong Major Project of Basic and Applied Basic Research No. 2020B0301030008.

Data Availability Statement This manuscript has no associated data or the data will not be deposited. [Authors' comment: This is a theoretical study and no experimental data has been listed.]

References

1. F. Karsch, Nucl. Phys. A **698**, 199 (2002). https://doi.org/10.1016/S0375-9474(01)01365-3
2. C.-Y. Wong, *Introduction to High-Energy Heavy-Ion Collisions* (WORLD SCIENTIFIC, 1994). https://doi.org/10.1142/1128
3. E. Shuryak, Rev. Mod. Phys. **89**, 035001 (2017). https://doi.org/10.1103/RevModPhys.89.035001
4. P. Braun-Munzinger, V. Koch, T. Schäfer, J. Stachel, Phys. Rep. **621**, 76 (2016). https://doi.org/10.1016/j.physrep.2015.12.003
5. J. Chen, D. Keane, Y.-G. Ma, A. Tang, Z. Xu, Phys.Rep. **760**, 1 (2018). https://doi.org/10.1016/j.physrep.2018.07.002
6. S. Wu, C. Shen, H. Song, Chin. Phys. Lett. **38**, 081201 (2021). https://doi.org/10.1088/0256-307X/38/8/081201
7. C. Shen, Y. Li, Nucl. Sci. Tech. **31**, 122 (2020). https://doi.org/10.1007/s41365-020-00829-z
8. K. Fukushima, C. Sasaki, Progress Particle Nucl. Phys. **72**, 99 (2013). https://doi.org/10.1016/j.ppnp.2013.05.003
9. A. Bzdak, S. Esumi, V. Koch, J. Liao, M. Stephanov, N. Xu, Phys. Rep. **853**, 1 (2020). https://doi.org/10.1016/j.physrep.2020.01.005
10. J. Adam et al., (STAR Collaboration). Phys. Rev. C **99**, 064905 (2019). https://doi.org/10.1103/PhysRevC.99.064905
11. J.-H. Gao, G.-L. Ma, S. Pu, Q. Wang, Nucl. Sci. Tech. **31**, 90 (2020). https://doi.org/10.1007/s41365-020-00801-x
12. Z.-B. Tang, W.-M. Zha, Y.-F. Zhang, Nucl. Sci. Tech. **31**, 81 (2020). https://doi.org/10.1007/s41365-020-00785-8
13. Z. Han, B. Chen, Y. Liu, Chin. Phys. Lett. **37**, 112501 (2020). https://doi.org/10.1088/0256-307x/37/11/112501
14. H. Wang, J.H. Chen, Y.G. Ma et al., Nucl. Sci. Tech. **30**, 185 (2019). https://doi.org/10.1007/s41365-019-0706-z
15. Y.-C. Liu, X.-G. Huang, Nucl. Sci. Tech. **31**, 56 (2020). https://doi.org/10.1007/s41365-020-00764-z
16. K.-J. Sun, L.-W. Chen, C.M. Ko, J. Pu, Z. Xu, Phys. Lett. B **781**, 499 (2018). https://doi.org/10.1016/j.physletb.2018.04.035
17. N. Yu, D. Zhang, X. Luo, Chin. Phys. C **44**, 014002 (2020). https://doi.org/10.1088/1674-1137/44/1/014002
18. X.G. Deng, Y.G. Ma, Phys. Lett. B **808**, 135668 (2020). https://doi.org/10.1103/PhysRevC.99.064905
19. H. Liu, D. Zhang, S. He, K.-J. Sun, N. Yu, X. Luo, Phys. Lett. B **805**, 135452 (2020). https://doi.org/10.1016/j.physletb.2020.135452
20. K.-J. Sun, L.-W. Chen, C.M. Ko, Z. Xu, Phys. Lett. B **774**, 103 (2017). https://doi.org/10.1016/j.physletb.2017.09.056
21. E. Shuryak, J.M. Torres-Rincon, Phys. Rev. C **100**, 024903 (2019). https://doi.org/10.1103/PhysRevC.100.024903
22. E. Shuryak, J.M. Torres-Rincon, Euro. Phys. J. A **56**, 241 (2020). https://doi.org/10.1140/epja/s10050-020-00244-3
23. A. Andronic, P. Braun-Munzinger, D. Gündüz, Y. Kirchhoff, M. Köhler, J. Stachel, M. Winn, Nucl. Phys. A **1010**, 122176 (2021). https://doi.org/10.1016/j.nuclphysa.2021.122176

24. D.-F. Wang, S. Zhang, Y.-G. Ma, Phys. Rev. C **101**, 034906 (2020). https://doi.org/10.1103/PhysRevC.101.034906
25. B.I. Abelev et al., STAR Collaboration. Phys. Rev. C **79**, 034909 (2009). https://doi.org/10.1103/PhysRevC.79.034909
26. R. Mattiello, H. Sorge, H. Stöcker, W. Greiner, Phys. Rev. C **55**, 1443 (1997). https://doi.org/10.1103/PhysRevC.55.1443
27. T.Z. Yan, Y.G. Ma, X.Z. Cai et al., Phys. Lett. B **638**, 50 (2006). https://doi.org/10.1016/j.physletb.2006.05.018
28. S. Zhang, J.H. Chen, H. Crawford, D. Keane, Y.G. Ma, Z. Xu, Phys. Lett. B **684**, 224 (2010). https://doi.org/10.1016/j.physletb.2010.01.034
29. S. Cho, T. Hyodo, D. Jido et al., Progress Particle Nucl. Phys. **95**, 279 (2017). https://doi.org/10.1016/j.ppnp.2017.02.002
30. T.T. Wang, Y.G. Ma, Eur. Phys. J. A **55**, 102 (2019). https://doi.org/10.1140/epja/i2019-12788-0
31. W. Zhao, C. Shen, C.M. Ko, Q. Liu, H. Song, Phys. Rev. C **102**, 044912 (2020). https://doi.org/10.1103/PhysRevC.102.044912
32. K.-J. Sun, C.M. Ko, B. Dönigus, Phys. Lett. B **792**, 132 (2019). https://doi.org/10.1016/j.physletb.2019.03.033
33. P. Danielewicz, G. Bertsch, Nucl. Phys. A **533**, 712 (1991). https://doi.org/10.1016/0375-9474(91)90541-D
34. D. Oliinychenko, L.-G. Pang, H. Elfner, V. Koch, Phys. Rev. C **99**, 044907 (2019). https://doi.org/10.1103/PhysRevC.99.044907
35. K.-J. Sun, R. Wang, C.M. Ko, Y.-G. Ma, C. Shen, arXiv e-prints , arXiv:2106.12742 (2021)
36. Z.-W. Lin, C.M. Ko, B.-A. Li, B. Zhang, S. Pal, Phys. Rev. C **72**, 064901 (2005). https://doi.org/10.1103/PhysRevC.72.064901
37. F. Bellini, A.P. Kalweit, Phys. Rev. C **99**, 054905 (2019). https://doi.org/10.1103/PhysRevC.99.054905
38. S. Huang, Z. Chen, W. Li, J. Jia, Phys. Rev. C **101**, 021901 (2020). https://doi.org/10.1103/PhysRevC.101.021901
39. M. Sievert, J. Noronha-Hostler, Phys. Rev. C **100**, 024904 (2019). https://doi.org/10.1103/PhysRevC.100.024904
40. J.L. Nagle, A. Adare, S. Beckman, T. Koblesky, J.O. Koop, D. McGlinchey, P. Romatschke, J. Carlson, J.E. Lynn, M. McCumber, Phys. Rev. Lett. **113**, 112301 (2014). https://doi.org/10.1103/PhysRevLett.113.112301
41. S.H. Lim, J. Carlson, C. Loizides, D. Lonardoni, J.E. Lynn, J.L. Nagle, J.D. Orjuela Koop, J. Ouellette, Phys. Rev. C **99**, 044904 (2019). https://doi.org/10.1103/PhysRevC.99.044904
42. R. Katz, C.A.G. Prado, J. Noronha-Hostler, A.A.P. Suaide, Phys. Rev. C **102**, 041901 (2020). https://doi.org/10.1103/PhysRevC.102.041901
43. S. Zhang, Y.G. Ma, G.L. Ma, J.H. Chen, Q.Y. Shou, W.B. He, C. Zhong, Phys. Lett. B **804**, 135366 (2020). https://doi.org/10.1016/j.physletb.2020.135366
44. P. Liu, J.-H. Chen, Y.-G. Ma et al., Nucl. Sci. Tech. **28**, 55 (2017). https://doi.org/10.1007/s41365-017-0207-x
45. X.-N. Wang, M. Gyulassy, Phys. Rev. D **44**, 3501 (1991). https://doi.org/10.1103/PhysRevD.44.3501
46. M. Gyulassy, X.-N. Wang, Comput. Phys. Commun. **83**, 307 (1994). https://doi.org/10.1016/0010-4655(94)90057-4
47. B. Zhang, Comput. Phys. Commun. **109**, 193 (1998). https://doi.org/10.1016/S0010-4655(98)00010-1
48. B.-A. Li, C.M. Ko, Phys. Rev. C **52**, 2037 (1995). https://doi.org/10.1103/PhysRevC.52.2037
49. G.-L. Ma, Z.-W. Lin, Phys. Rev. C **93**, 054911 (2016). https://doi.org/10.1103/PhysRevC.93.054911
50. Z.-W. Lin, L. Zheng, Nucl. Sci. Tech. **32**, 113 (2021). https://doi.org/10.1007/s41365-021-00944-5
51. L. Csernai, J.I. Kapusta, Phys. Rep. **131**, 223 (1986). https://doi.org/10.1016/0370-1573(86)90031-1
52. L.-W. Chen, C. Ko, B.-A. Li, Nucl. Phys. A **729**, 809 (2003). https://doi.org/10.1016/j.nuclphysa.2003.09.010
53. W. Zhao, L. Zhu, H. Zheng, C.M. Ko, H. Song, Phys. Rev. C **98**, 054905 (2018). https://doi.org/10.1103/PhysRevC.98.054905
54. K.-J. Sun, C.M. Ko, Z.-W. Lin, Phys. Rev. C **103**, 064909 (2021). https://doi.org/10.1103/PhysRevC.103.064909
55. K.-J. Sun, L.-W. Chen, Phys. Lett. B **751**, 272 (2015). https://doi.org/10.1016/j.physletb.2015.10.056
56. L. Adamczyk et al., STAR Collaboration. Phys. Rev. C **96**, 044904 (2017). https://doi.org/10.1103/PhysRevC.96.044904
57. D. Zhang, Nucl. Phys. A **1005**, 121825 (2021). https://doi.org/10.1016/j.nuclphysa.2020.121825
58. S. Zhang, Y.H. Zhu, G.L. Ma, Y.G. Ma, X.Z. Cai, J.H. Chen, C. Zhong, Nucl. Phys. A **860**, 76 (2011). https://doi.org/10.1016/j.nuclphysa.2011.05.008
59. P. Braun-Munzinger, K. Redlich, J. Stachel, Particle production in heavy ion collisions, in *Quark-Gluon Plasma 3* (World Scientific Publishing Co Pte Ltd, 2004) pp. 491–599. https://doi.org/10.1142/9789812795533_0008
60. D. Zhang, (for the STAR Collaboration), JPS Conf. Proc. **32**, 010069 (2019). https://doi.org/10.7566/JPSCP.32.010069
61. N. Yu, X. Luo, Eur. Phys. J. A **55**, 26 (2019). https://doi.org/10.1140/epja/i2019-12691-8
62. V. Vovchenko, B. Dönigus, B. Kardan, M. Lorenz, H. Stoecker, Phys. Lett. B **809**, 135746 (2020). https://doi.org/10.1016/j.physletb.2020.135746
63. K.-J. Sun, L.-W. Chen, Phys. Rev. C **95**, 044905 (2017). https://doi.org/10.1103/PhysRevC.95.044905
64. N. Shah, Y.G. Ma, J.H. Chen, S. Zhang, Phys. Lett. B **754**, 6 (2016). https://doi.org/10.1016/j.physletb.2016.01.005
65. A. Andronic, P. Braun-Munzinger, K. Redlich, J. Stachel, Nature **561**, 321 (2018). https://doi.org/10.1038/s41586-018-0491-6
66. K.-J. Sun, L.-W. Chen, Phys. Rev. C **93**, 064909 (2016). https://doi.org/10.1103/PhysRevC.93.064909
67. S. Sombun, K. Tomuang, A. Limphirat, P. Hillmann, C. Herold, J. Steinheimer, Y. Yan, M. Bleicher, Phys. Rev. C **99**, 014901 (2019). https://doi.org/10.1103/PhysRevC.99.014901
68. M. Aggarwal *et al.* (STAR collaboration), arXiv e-prints , arXiv:1007.2613 (2010)